Title: Development and Characterization of a Miniaturized, Low-cost Cross-flow Direct Evaporative Cooler

Authors: Olivia M. Reynolds,[a] David B. Thiessen,[a] and Bernard J. Van Wie[a]

[a]Gene and Linda Voiland School of Chemical Engineering and Bioengineering, Washington State University, Pullman, WA 99164-6505, United States of America

Emails:
Reynolds: olivia.ranft@wsu.edu
Thiessen: thiessen@wsu.edu
Van Wie: bvanwie@wsu.edu

Corresponding author: Olivia M. Reynolds

Abstract
Evaporative cooling is a complex heat and mass transfer phenomenon with industrial and residential applications. We present the development of a miniaturized, very low-cost cross-flow direct evaporative cooler with potential applications as a teaching tool and as a laboratory testing apparatus for rapid, preliminary studies. We evaluate the impact of water flow rate, air velocity, and initial water temperature on air and water-side performance, including the cooling rate and efficiency, through comparison to theoretical results obtained using a newly developed, simple steady-state numerical model with a single fitting parameter and through regression analysis of a central composite fractional factorial design. The miniaturized device can be used to achieve water cooling rates up to 740 W, and air- and water side efficiencies of up to 80% and 23%, respectively, all of which were found to be strongly dependent on operating parameters and to vary with similar trends reported in existing studies on larger systems. Moreover, the numerical model can be used to predict outlet water temperatures, outlet air temperatures, cooling rates, and water-side efficiencies with average errors of 1%, 4%, 7%, and 11%, respectively, over a wide range of operating conditions. Results provide strong evidence that the miniaturized, low-cost evaporative cooler and associated model have potential for use in teaching or laboratory training and testing packing material applications.

Keywords: direct evaporative cooling, numerical model, factorial design, heat transfer, mass transfer

1. Introduction

Evaporative cooling is a critical and complex heat and mass transfer phenomenon widely utilized to reject heat in industrial processes in units such as cooling towers and as a lower-cost, environmentally friendly alternative to traditional air cooling processes in hot and dry climates [1]. Direct evaporative cooling, where water and air contact in either a counter-flow or cross-flow arrangement, involves coupled heat and mass transfer processes at the air-water interface resulting in sensible and latent heat transfer and air humidification as water evaporates. Depending on the process purpose, either the water, air, or both phases are cooled. Although evaporative cooling is widely used in industry, it has been cited as a phenomenon poorly understood by engineering students due to its complex nature [2], leaving them ill-equipped to manage evaporative cooling processes after entering industry. Simple experiments have been designed to foster students' understanding of evaporative cooling, such as an activity where students build and test a swamp cooler constructed from household materials [3], and observational experiments where students blow on their skin wetted by water or alcohol and observe temperature changes [4]. However, we are aware of no examples of low-cost, robust, industrially-relevant learning tools that have been constructed to demonstrate evaporative cooling in detail. We have previously demonstrated that visual hands-on learning tools demonstrating fluid mechanics and heat transfer processes can improve conceptual understanding of underlying principles [4-6]; thus, opportunities for hands-on investigations with classroom-appropriate evaporative cooling systems may help prepare students for work in industry. Further, the multitude of factors affecting the performance of evaporative coolers, including air and water-side temperatures, flow rates, air humidity, and geometric parameters and material properties of packing medium make experimental studies critically important to the understanding of how to best optimize these systems. However, laboratory-scale evaporative cooling apparatuses are often costly, and cumbersome to alter. Low-cost, miniaturized, simple systems that behave similarly to larger scale prototypes would provide opportunities for rapid, preliminary testing of new packing materials, flow configurations, and of the influence of operating parameters.

Due to the critical importance of evaporative cooling processes, there is extensive literature focused on development of models to predict performance. Kloppers and Kroger [7] provide a detailed explanation and comparison of three models traditionally used to predict cooling tower performance: the Merkel, e-NTU, and Poppe methods. The former two rely on several simplifying assumptions to predict cooling tower performance including assuming saturated outlet air, neglecting the change in water flow rate due to evaporation, and that the relative rates of heat and mass transfer are equal, i.e., the Lewis factor is equal to one. Poppe relaxed these assumptions, resulting in improved prediction of parameters including the heat rejection rate. The classical models are useful for predicting the performance of large-scale cooling towers, but do not consider temperature variations between the bulk water and surface, effects of the velocity profile in the water film, or influences of packing geometry. To address these shortcomings, alternative numerical models for evaporative coolers with film-type flow have been developed. Fisenko and Petruchik [8] developed a set of differential equations to predict the change in film thickness, water film temperature, and air temperature in a film-flow counter flow cooling tower and utilized empirical correlations to calculate heat and mass transfer coefficients; however they only considered temperature variations in the flow direction. Dai and Sumathy [9] modeled air and interface temperatures in a cross-flow air-cooling device utilizing a surface energy balance, average water velocity, an empirical correlation for the evaporation rate of water, a function of the wet-bulb heat transfer coefficient for heat transfer from a wet surface related to the sensible heat transfer coefficient and the latent heat, and a fitting parameter to account for unwetted portions of packing. They do not report water temperature variations across the liquid film. Kovačević and Sourbron [10] modeled air-side temperature profiles in a cross-flow evaporative cooler operating at steady-state with a constant water temperature using empirical heat and mass transfer correlations for flow between parallel plates. Finally, Ibrahim, Nabham, and Anabtawi [11] modeled temperature variations within a falling liquid film in a counterflow cooling tower considering velocity variations within the film. However, their model incorporates the Lewis factor and Merkel tower characteristic group, which are not geometry-specific, rather than air-side empirical heat and mass transfer coefficients for heat and mass transfer at the interface. To our knowledge, there are no existing numerical models which allow estimation of water-side temperature profiles and overall performance for cross-flow evaporative coolers, incorporate velocity distributions in the water film, and make use of easily estimable geometry-specific parameters.

In addition to numerical investigation, numerous experimental studies have been completed on evaporative cooling systems, including those focused on packing arrangement [12, 13], testing of novel packing materials including natural plant materials such as bulrush [14], porous cylinders incorporating rice bran [15], and spindle-shaped hollow fibers [16], and the impact of one or several operating parameters on cooling tower or air-cooling performance. Tejero-Gonzáleza and Franco-Salas [17] recently provided an extensive review of studies on direct evaporative air coolers with wetted pads, and the impact of parameters such as air and water flow-rates and water temperature are commonly studied in cooling towers [18, 19]. Most studies in existing literature are investigations of performance with a single factor varied at a time, with few investigating potential interactions between operating parameters. Response surface methodology (RSM) provides an alternative to traditional testing, allowing a more complete understanding of the cooperative effects of operating parameters [20]. To our knowledge, relatively few examples of RSM studies to optimize cooling tower performance exist. Ramakrishnan and Arumugam [21] developed a regression model for the impact of air and water flow rate, inlet water temperature, and packing height, on the outlet water temperature in a forced draft evaporative cooler with wire mesh fill and demonstrated non-linear and interacting effects. Javadpour et.al. [22] used RSM to optimize the flow rate and nanoparticle concentration of carbon nanotubes to provide the maximum temperature change and efficiency in a cross-flow cooling tower utilizing nanofluid as a working fluid, again noting several significant interactions between parameters. The extensive interest represented in the literature in evaporative cooling technology demonstrates the need to develop simple experimental systems allowing low-cost and rapid experimentation and which utilize experimental methods to allow identification of parameter interactions and performance optimization of multiple operating parameters.

We report the development and characterization of a miniaturized, flexible, low-cost direct evaporative cooler with several potential applications including use as a teaching module to allow students to gain hands-on experience with evaporative cooling devices, or for use in preliminary laboratory testing where the use of larger scale evaporative cooling systems is not feasible. We present the results of the impact of water flow rate, air velocity, and initial water temperature on the air- and water-side cooling efficiencies and the cooling rate, assessed through a central composite fractional factorial design and response surface equations, allowing investigation of synergistic and antagonistic interactions between operating parameters. In addition, we develop and assess the validity of a steady-state two-dimensional numerical model with a single fitting parameter for prediction of the water-side temperature profile,

outlet air conditions, and overall performance, which makes use of empirical correlations for air-side convective heat and mass transfer coefficients. This model considers temperature and velocity variations perpendicular to the flow direction in the water film and geometric characteristics of the packing. The use of familiar governing differential equations for heat transfer and empirical correlations for heat and mass transfer typically encountered in engineering courses may make this model palatable to undergraduate students and help further their understanding of fundamental evaporative cooling phenomena. We believe that the evaporative cooler developed herein will be useful in a number of classroom and technical settings to allow simple, low-cost experimentation.

2. Theory and Calculations

2.1 Model geometry and simplifying assumptions

A two-dimensional numerical model to approximate the heat and mass transfer behavior in the evaporative cooling device through expanded aluminum, clay-coated mesh packing used in our experiments with approximate geometry shown in Figure 1A was developed. The model was used to predict the liquid-side temperature profile with variations in the flow direction and across the thickness of the liquid film flowing down the packing material considered. Additionally, bulk outlet air conditions and overall performance were predicted. The finite difference approach was utilized to predict liquid-side temperature profiles within the water film, air-side empirical heat and mass transfer correlations were used to estimate interfacial heat and mass transfer from water to air, and an overall enthalpy balance was used to predict air outlet conditions. For simplicity, directional changes in the water flow due to mesh geometry and mixing at the intersecting points of the mesh were ignored. For prediction of the water-side temperature profiles, water was modeled as multiple, individual, rectangular rivulets with a constant thickness flowing at a fixed downwards angle with a width equal to the mesh thickness and height equal to the total flow distance. On the air-side, we assumed that air flow was perpendicular to water rivulets and approximated rivulet geometry as cylindrical with a diameter equal to the mesh thickness for interfacial heat and mass transfer calculations. Geometry utilized in the model is shown in Figure 1B.

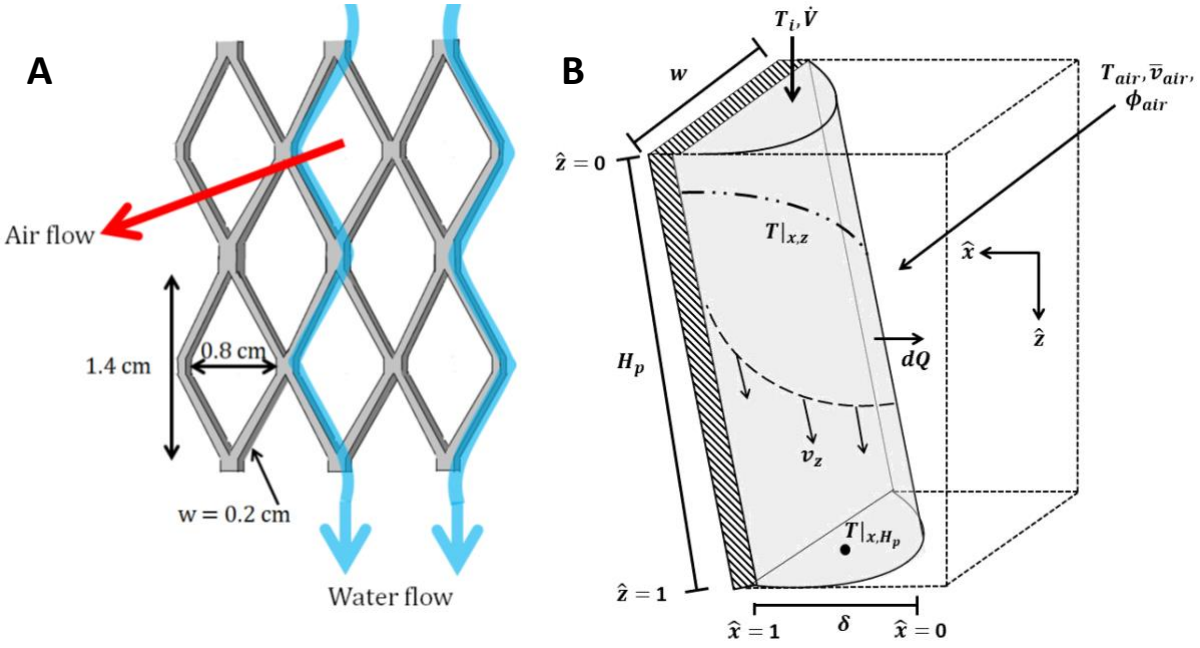

Figure 1. Diagram of subsection of expanded aluminum wire mesh packing with air and water flow directions (A); simplified geometry used for finite difference model (B).

The following simplifying assumptions are used in the overall model: 1) the system is at steady state; 2) water flow can be modeled as laminar film flow; convection dominates conduction in the flow direction; 3) the superficial air velocity is uniform throughout the packing and can be represented by the average velocity measured at the packing outlet; 4) the air-side temperature and relative humidity (ϕ_{air}) can be represented by bulk-average values, i.e., variation in the air flow direction is not considered; and 5) air-side heat and mass transfer coefficients can be estimated from empirical correlations for flow past a single cylinder alone, and that any effects of heat and mass transfer arising from the overall packing geometry are neglected. Supersaturated air conditions are not considered.

Model inputs include water flow rate, air velocity, inlet air and water temperatures, inlet relative humidity, and packing dimensions.

2.2 Velocity profile of liquid rivulets

The velocity profile of the water traveling down the medium is modeled as a rectangular falling film down a tilted flat plate. The thickness of the rivulet, δ, can be estimated from the total volumetric flowrate as shown in Eqn. 1, where μ and ρ are the viscosity and density of the water respectively, w the width of the rivulet, assumed equal to the width of a single layer of packing medium, 0.002 m, $\dot{V}_l$ the volumetric flow rate of the water, β the angle from vertical at which the rivulet flows, estimated as 29.7 ° from the packing dimensions, and N_c is the number of channels for water flow, a fitting parameter which was estimated by minimizing the sum of squares error between experimentally measured and predicted heat transfer rates:

$$\delta = \left(\frac{3\mu\dot{V}_l}{\rho g cos\ (\beta) N_c w}\right)^{1/3} \tag{1}$$

The velocity at any horizontal position in the falling rivulet is then estimated with Eqn. 2:

$$v_z = \frac{g\rho\delta^2 cos\ (\beta)}{2\mu}(1-\hat{x}^2) = v_{z,max}(1-\hat{x}^2) \tag{2}$$

2.3 Air-side heat and mass transfer coefficients

Since we are assuming air flows perpendicularly over individual, semi-cylindrical water rivulets on both sides of a single thin strip of aluminum packing material, the heat and mass transfer coefficients on the air-side are approximated using empirical correlations for flow past a cylinder with physical properties evaluated at the bulk-average air temperature and relative humidity. The convective heat transfer coefficient is calculated using the Nusselt number correlation in Eqn. 3, valid for Reynolds numbers of 40-4,000 [23], where k_a is the thermal conductivity of the air, and Re and Pr the Reynolds and Prandtl numbers, respectively:

$$Nu = \frac{h_o w}{k_a} = 0.683 Re^{0.466} Pr^{1/3} \tag{3}$$

The molar flux of water vapor at the interface, used to estimate latent heat transfer, is calculated using the difference between the water vapor pressure at the interface temperature and bulk air temperature, where ϕ_{air} is the relative humidity, multiplied by the mass transfer coefficient, k_g:

$$N_l = k_g\left(P_{vap}|_{T=T_s} - \phi_{air} P_{vap}|_{T=T_{air}}\right) \tag{4}$$

The vapor pressure at the surface temperature and bulk air temperature are estimated using Antoine's equation using the surface temperature along the height of the packing and the bulk-average air temperature, respectively. The mass transfer coefficient, k_c' , used in combination with a molar concentration driving force in the molar flux equation, is calculated using the Colburn J-factor correlation in Eqn. 5 [24], where Sc is the Schmidt number ($Sc = \mu/\rho D_{wa}$) and D_{wa} the diffusivity of water in air:

$$J_D = \frac{k_c'}{\bar{v}_{air}} Sc^{2/3} = 0.6 Re^{-0.487} \tag{5}$$

The coefficient, k_c', can be related to a mass transfer coefficient, k_g, appropriate for use with a vapor pressure driving force in the molar flux equation and estimated as follows in Eqn. 6:

$$k_g = \frac{0.6\bar{v}_{air}}{Re^{0.487} Sc^{2/3} RT} \tag{6}$$

2.4 Liquid-side temperature

The liquid side temperature profile is predicted with the finite difference approach. For convenience, the horizontal (x) and vertical position (z) in water rivulets, as well as the water temperature, are made dimensionless as follows in

Eqns. 7a-7c, where H_p is the total packing height, and T, T_i, and T_{ai} the temperature of the water at any position, the inlet temperature of the water, and the inlet temperature of the air, respectively.

$$\hat{x} = \frac{x}{\delta} \quad (a) \qquad \hat{z} = \frac{z\cos(\beta)}{H_p} \quad (b) \qquad \hat{T} = \frac{T - T_i}{T_{ai} - T_i} \quad (c) \qquad (7)$$

Heat transfer for laminar flow can be modeled for a single water rivulet as it flows down the packing with Eqn. 8, where $\alpha = k_l/\rho C_p$:

$$v_z \frac{\partial \hat{T}}{\partial \hat{z}} = \frac{\alpha H_p}{\cos(\beta)\delta^2} \frac{\partial^2 \hat{T}}{\partial \hat{x}^2} \qquad (8)$$

The temperature at the top of the rivulet is assumed fixed and equal to the inlet water temperature. An insulating boundary is assumed at the packing-water interface, and the temperature gradient at the air-water interface is assumed to be a function of the surface temperature, resulting in the following dimensionless boundary conditions in Eqns. 9a-9c:

$$\hat{T}|_{\hat{z}=0} = 0 \quad (a) \qquad \left.\frac{\partial \hat{T}}{\partial \hat{x}}\right]_{\hat{x}=1} = 0 \quad (b) \qquad \left.\frac{\partial \hat{T}}{\partial \hat{x}}\right]_{\hat{x}=0} = f(\hat{T}_s) \quad (c) \qquad (9)$$

Eqn. 8 can be rewritten in finite difference form as follows, where $\Delta\hat{x}$ and $\Delta\hat{z}$ are the step sizes in the horizontal and vertical directions, respectively, and λ is a dimensionless group, defined in Eqn. 11.

$$\hat{T}|_{\hat{x},\hat{z}} - \hat{T}|_{\hat{x},\hat{z}-\Delta\hat{z}} = \lambda\left(\hat{T}|_{\hat{x}+\Delta\hat{x},\hat{z}} - 2\hat{T}|_{\hat{x},\hat{z}} + \hat{T}|_{\hat{x}-\Delta\hat{x},\hat{z}}\right) \qquad (10)$$

$$\lambda = \frac{\alpha H_p \Delta\hat{z}}{\delta^2 v_{z,max}(1-\hat{x}^2)\Delta\hat{x}^2} \qquad (11)$$

The surface temperature of the falling film is estimated using an energy balance at the interface between the air and water, shown in Eqn. 12, accounting for sensible and latent heat transfer across the boundary, where M_l is the molecular weight of water and ΔH_{vap} the heat of vaporization evaluated at the inlet water temperature:

$$k_w \frac{\partial \mathrm{T}}{\partial \mathrm{x}}|_{x=0,z} = h_o\left(T|_{x=0,z} - T_a\right) + M_l N_l \Delta H_{vap} \qquad (12)$$

Eqns. 9a, 9a, 10, and 12 were solved simultaneously to estimate the dimensionless temperature at the boundaries and all interior node points of the finite difference grid using step sizes of $\Delta\hat{z} = 0.01$ ($n_z = 100$) and $\Delta\hat{x} = 0.05$ ($n_x = 20$).

2.5 Estimation of air-side outlet conditions

To estimate the outlet air temperature and relative humidity and thus, the bulk average values for use in the molar flux and sensible heat transfer rates, a macroscopic enthalpy balance on the air as shown in Eqn. 13 is used, where $\dot{m}_a$ is the mass flow rate of dry air, $H_{ma,out}$ and $H_{ma,in}$ the enthalpies of moist air at the inlet and outlet conditions, calculated with Eqn. 14, and $\dot{Q}_l$ and $\dot{Q}_s$ the latent and sensible heat transferred at the air-water interface:

$$\dot{m}_a H_{ma,out} = \dot{m}_a H_{ma,in} + \dot{Q}_s + \dot{Q}_l \qquad (13)$$

The enthalpy of moist air per kilogram dry air is estimated with Eqn. 14, where ω is the humidity ratio in kg H_2O/kg dry air and $\Delta H_{vap,ref}$ the heat of vaporization evaluated at 0 °C:

$$H_{ma} = c_{p,a} T_a + \omega(\Delta H_{vap,ref} + c_{pv} T_a) \qquad (14)$$

The total sensible heat transferred from the interface to the air along the packing height is calculated with Eqn. 15:

$$\dot{Q}_s = \sum_{i=1}^{n_z} h_o N_c w H_p \Delta\hat{z}\left(T|_{x=0,z_i} - T_a\right) \tag{15}$$

The outlet humidity ratio is calculated as the sum of the inlet humidity ratio plus the water evaporation rate on a basis of one kilogram dry air as shown in Eqn. 16:

$$\omega_{out} = \omega_{in} + \frac{\sum_{i=1}^{n_z} k_g M_l N_c w H_p \Delta\hat{z}\left(P_{vap}|_{T_{s,i}} - \phi_{air} P_{vap}|_{T_{air}}\right)}{\dot{m}_a cos\,(\beta)} \tag{16}$$

Finally, the latent heat entering the bulk air from the interface is calculated with Eqn. 17, where H_v is the enthalpy of water vapor, calculated with Eqn. 18:

$$\dot{Q}_L = \sum_{i=1}^{n_z} \frac{k_g M_l N_c w H_p \Delta\hat{z}\left(P_{vap}|_{T_{s,i}} - \phi_{air} P_{vap}|_{T_{air}}\right) H_v}{cos\,(\beta)} \tag{17}$$

$$H_v = c_{pv} T_s + \Delta H_{vap,ref} \tag{18}$$

Equations 13-18 are solved to determine the outlet air temperature satisfying the air-side enthalpy balance.

2.6 Estimation of water- and air-side performance

The air-side and water-side efficiency of the direct evaporative cooler, a measure of how effectively air or water is cooled in a single pass through the cooler relative to the incoming air wet-bulb temperature, are calculated as follows, where $T_{i,db}$ and $T_{o,db}$ are the dry-bulb temperatures of the incoming and outgoing air, $T_{i,wb}$ is the wet-bulb temperature of the incoming air, and $T_{w,out}$ is the outlet temperature of the water:

$$\varepsilon_{air} = 100 \cdot \frac{T_{i,db} - T_{o,db}}{T_{in,db} - T_{i,wb}} \tag{19}$$

$$\varepsilon_{water} = 100 \cdot \frac{T_i - T_{w,out}}{T_i - T_{i,wb}} \tag{20}$$

Because water cooling trials were completed in non-steady state conditions, the experimental water-side efficiency was averaged for the first 30 s of operation. The efficiency predicted by the finite difference model was calculated using the predicted velocity-weighted average outlet temperature at the third experimental time-point. The initial cooling rate, a measure of how quickly heat is transferred from the water to the air when the water is hottest and therefore the maximum temperature and vapor pressure driving forces exist at the interface, was calculated for experimental data as shown in Eqn. 21, where m_w is the total mass of water, $c_{p,w}$ the heat capacity, Δt the time between the initial and final temperature measurement, chosen as 60 s for all trials as the temperature change was approximately linear over this region, and ΔT_w the temperature change of the water measured in the reservoir:

$$\dot{Q}_w = \frac{m_w c_{p,w} \Delta T_w}{\Delta t} \tag{21}$$

The steady-state heat transfer rate predicted by the experimental model was estimated by integrating the heat flux over the surface area of a single rivulet and multiplying by the number of rivulets, resulting in Eqn. 22:

$$\dot{Q}_w = \frac{N_c w k_w (T_a - T_i) H_p \Delta\hat{z}}{\delta \Delta\hat{x}} \sum_{i=1}^{n_z} \left(T|_{\Delta\hat{x},z_i} - T|_{0,z_i}\right) \tag{22}$$

3. Methods

3.1 Experimental apparatus

The miniature, cross-flow direct evaporative cooler shown in Figure 2A was used for all laboratory experiments. The 12.4 x 22.5 x 3.18 cm frame was laser cut from 0.32 cm thick acrylic and assembled with acrylic cement. The back plate had a square opening to allow air inflow and the front plate had six 1.75 cm wide slotted openings for outflow. The bottom 5 cm of the frame acted as a collection reservoir to capture water after it flowed through the medium with a 2.54 cm diameter hole to allow for drainage back to the main reservoir. A 12 V DC 11.9 cm square fan (Figure 2C) was secured to the housing on the back plate to provide airflow across a 11.5 x 11.5 x 2 cm section of commercially available expanded aluminum, clay-coated humidifier medium (Figure 2B) which was inserted between the front and back frame plates. Water was distributed via a 14 cm long, 0.63 cm inside diameter polycarbonate tube with 0.16 cm diameter holes spaced 1.5 cm apart in two offset rows. A 12 V, 4W battery-powered centrifugal pump was used to circulate water from a one liter reservoir to the distributor. The air velocity and water flow rate were controlled by varying the input voltage supplied from 18 V DC power supplies. Air velocity at the outlet of the packing was correlated to the voltage supplied by first utilizing a pitot tube to measure the difference between the stagnation pressure at the tip of the tube and ambient static pressure at various voltages. The pitot tube was instrumented with a calibrated Validyne DP103-08 pressure sensor with a range of 55 Pa and placed at the outlet of a fairly open flow channel. Measured pressure differentials were converted to velocity. The weighted average velocity was then calculated for a fixed voltage across one-half of the packing surface by measuring the pressure differential every 2 mm, and was compared to the velocity measured for an open channel. The ratio between the weighted average and open-channel velocity was used to scale open-channel measurements at each experimental voltage. Water flow rate was correlated to voltage supplied by manually measuring the volume output over time at various voltages.

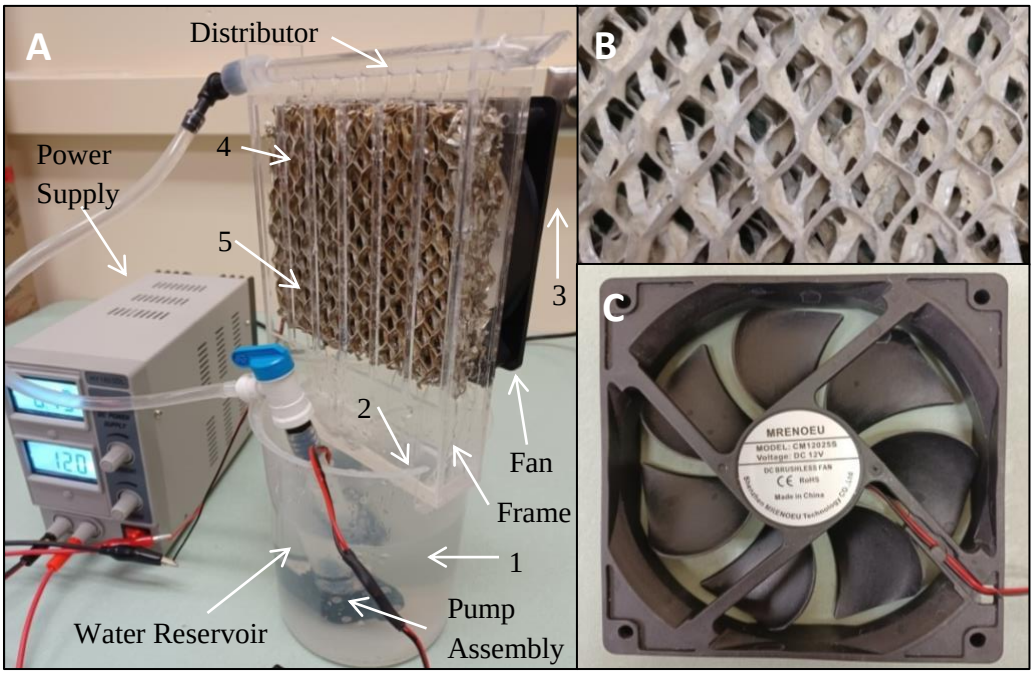

Figure 2. Experimental evaporative cooling apparatus with thermocouple locations indicated with numbers 1-5 (A), close-up of expanded aluminum evaporative cooling medium (B), and 12 V fan used to provide air flow (C).

Temperatures were recorded every second with calibrated type K thermocouples and a Huato S220-T8 8-channel data logger at five numbered locations labeled in Figure 2A: in the reservoir beaker (1), in the water at the bottom of the frame (2), approximately 2.5 cm from the fan inlet (3), and 0.64 cm from the medium outlet 2.54 cm from the top and 2.54 cm from the bottom (4 and 5).

3.2 Evaluation of air-side performance and impact of water flow rate and air velocity

To determine the effect of water flow rate and air velocity on the air-side efficiency, the cooler was operated in recycle mode with 900 mL of water until the water temperature reached a steady-state minimum near the wet-bulb

temperature. The superficial velocity measured at the packing outlet was varied from 0.14-1.6 m/s with a constant water flow rate of 24.7 mL/s then the water flow rate was varied from 12.5-31.8 mL/s with a constant air velocity of 0.7 m/s. The inlet air temperature and ambient relative humidity varied from 21.2-21.7 ºC and 25.9-27.9%, respectively, for trials with varying air velocity, and 21.3-21.7 º°C and 17.7-19.3% for trials with varying water flow rate. Temperatures were recorded for each voltage at the five locations detailed in Section 3.1 for five minutes with three experimental replicates.

3.3 Evaluation of impact of water flow rate, air velocity, and initial water temperature on cooler performance
To determine the impact of water flow rate, air velocity, and initial water temperature on the water-side performance, a three factor, five level circumscribed central composite fractional factorial design with experimental conditions and coded factorial design values shown in Table 1 was completed.

Table 1. Experimental conditions for fractional factorial design runs

Expt.	Respective scaled values	Pump voltage [V]	Fan voltage [V]	Water flow rate [mL/s]	Air velocity [m/s]	Initial temperature [°C]
1	(-1,-1, -1)	5.7	5	18.7	0.4	37
2	(1,-1,-1))	10.3	5	29.1	0.4	37
3	(-1, 1, -1)	5.7	10	18.7	1.0	37
4	(1, 1, -1)	10.3	10	29.1	1.0	37
5	(-1, -1, 1)	5.7	5	18.7	0.4	53
6	(1, -1, 1)	10.3	5	29.1	0.4	53
7	(-1, 1, 1)	5.7	10	18.7	1.0	53
8	(1, 1, 1)	10.3	10	29.1	1.0	53
9	(-1.682, 0, 0)	4.1	7.5	12.9	0.7	45
10	(1.682, 0, 0)	11.9	7.5	31.7	0.7	45
11	(0, -1.682, 0)	8	3.3	24.7	0.15	45
12	(0, 1.682, 0)	8	11.7	24.7	1.2	45
13	(0, 0, -1.682)	8	7.5	24.7	0.7	31.5
14	(0, 0, 1.682)	8	7.5	24.7	0.7	58.5
15-20	(0,0,0)	8	7.5	24.7	0.7	45

Fan and pump voltage were used as input parameters in the factorial design to ensure consistent factor settings between experiments as the air velocity and flow rate were difficult to measure. Pump and fan voltage were varied from 4.1 to 11.9 V and 3.3 to 11.7 V, corresponding to water flow rates of 12.9 to 31.7 mL/s and air velocities of 0.15 to 1.2 m/s, respectively, and initial water temperature was varied from 31.5 to 58.5 °C. The ambient temperature and inlet relative humidity varied from 21.3 to 21.9 °C and 27.5 to 29.5%, respectively, over all experiments, which were completed in a randomized order with six replicates at the center point. Temperatures were continuously recorded for 15 minutes at locations indicated in Figure 2A.

3.4 Statistical analysis and regression model generation
Multivariate linear regression with ANOVA was performed using R Version 4.1.2 by inputting the results of the fractional factorial design to quantify factors and factor interactions significantly affecting the initial cooling rate and the water-cooling efficiency. The scaled factorial values for each variable were used in the model to allow direct comparison of the magnitude of regression coefficients and the following model containing the presumed main effects, first order interactions, and quadratic polynomial terms for each factor and their combinations was used:

$$Output = a_0 P_v + a_1 F_v + a_2 T_i + a_{01} P_v F_v + a_{02} P_v T_i + a_{12} F_v T_i + a_{00} {P_v}^2 + a_{11} {F_v}^2 + a_{22} {T_i}^2$$

A reduced model was developed by employing a backwards elimination routine to sequentially eliminate terms from the full model with a p-value greater than 0.1 until all remaining terms were significant. The reduced model significance, lack-of-fit, and adjusted and predicted R^2 values, which represent the goodness-of-fit with consideration of the number of model terms and predictive power of the regression equation, respectively, were then determined, predicted output values were calculated for each experiment, and the percentage error between the measured and predicted values was evaluated.

4. Results and Discussion

4.1 Air-side performance of miniaturized evaporative cooler

While there was no effect of water flow rate on air outlet temperature or air-side cooling efficiency when the system was operated at steady-state with a minimized, constant water temperature, both the air-side cooling efficiency and outlet air temperature were strongly affected by the air-side velocity. A significant 16% decrease in the efficiency and a 1.7 °C increase in outlet air temperature was observed over the range of velocities tested, as shown in Figure 3B. The steady-state water temperature in all cases was constant at less than 1 °C above the wet-bulb temperature of the incoming air, which is the theoretical equilibrium temperature to which water can be cooled by evaporative cooling. At this temperature the partial pressure of water vapor at the interface matches that in the bulk air and the evaporation rate of water is zero; thus no further cooling of the water occurs. The air-side cooling efficiency was not affected by water flow rate under these conditions. Over the 12.5 mL/s to 31.8 mL/s water flow rate, air was cooled by 7.7 ± 0.3 °C on average and efficiencies varied by only 6.9%. No significant differences ($p = 0.89$) were detected for efficiency as a function of water flow rate. Conversely, the efficiency was significantly affected ($p = 8.7 \times 10^{-8}$) by the inlet air velocity and varied by 16.1% over the range of air velocities tested. The maximum average efficiency of 79.8% occurred at 0.14 m/s and a minimum of 63.6% occurred at 1.6 m/s, demonstrating an inverse relationship between velocity and efficiency. The air temperature decreased by an average of 8.0 °C at 0.3 m/s and by 6.4 °C at 1.6 m/s, again supporting improved performance at low velocities.

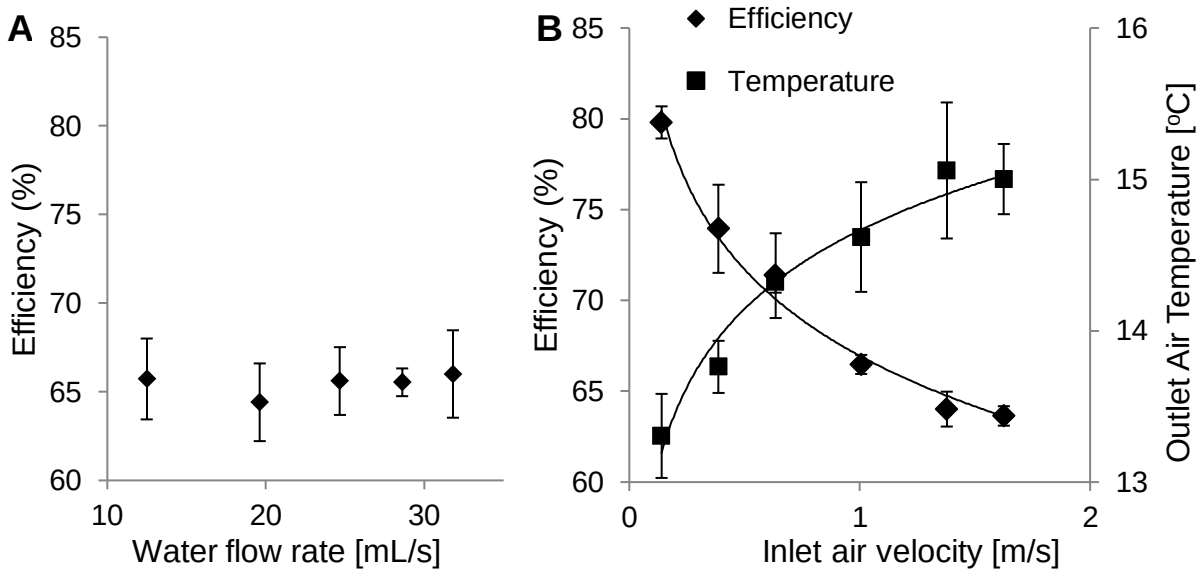

Figure 3. Air-side efficiency and outlet air temperature as functions of water flow rate (a) and inlet air velocity (b).

The non-linear increase in the outlet air temperature and decrease in efficiency can be explained considering the contact time between the water and air. As the velocity increases, the contact time for heat and mass transfer between the air and water reduces, leading to a lower temperature change on the air side and thus, a lower efficiency. As velocity continues to increase to very high values and contact time approaches zero, air will exit the packing at its inlet temperature, leading to a theoretical minimum efficiency. Increasing the velocity further above this will not lead to a further decrease in efficiency because the efficiency depends on the difference between incoming and outgoing air. To evaluate the performance of the low-cost, miniaturized evaporative cooler in light of larger laboratory systems, it is necessary to compare the influence of flow rate and velocity to trends reported in existing literature. Sheng and Nnanna [25] report an efficiency decrease of 19% over a 0.8-3 m/s air velocity range for a bench-scale direct evaporative cooler with cellulose paper medium and fit a non-linear empirical correlation showing that efficiency related to air velocity raised to the -0.19 power. Using a differential energy balance on air and turbulent heat transfer correlations, Wu, et.al. [26] derive a function for the efficiency in the form $\varepsilon_{air} = 1 - exp(-\beta \frac{\delta}{\bar{v}_{air}^{0.2}})$, where β is constant, and predict an approximately 16% decrease in efficiency for a 0.1 m thick fiberglass paper corrugated medium pad with an increase in velocity from 1 to 4 m/s. The measured change in

efficiency in our system of 16% over a 1.5 m/s range in air velocity is slightly larger than decreases previously reported in the literature, but the overall trend agrees well.

Regarding the influence of water flow rate, Nada, et.al. [27] report that the efficiency increased from 60-68% in a direct evaporative cooler constructed with a corrugated cellulose paper medium when water flow rate was varied from 46.7 to 167 mL/s with only a 2% increase between a 46.7 and 95.6 mL/s flowrate. In their review of evaporative cooling systems, Tejero-Gonzáleza and Franco-Salas [17] report a very weak dependence of the efficiency on water flow rate once the medium is fully wetted. These collective results along with our own for our miniature system are not surprising when one considers that for the air-side efficiency trials, the system was operated at steady-state with the average water temperature varying by only 0.25 °C across all flow rates, suggesting a constant surface temperature. At steady-state conditions where the water is near the wet-bulb temperature, the temperature is nearly uniform throughout the rivulet, so the water flow rate has minimal effect on heat transfer compared to situations with larger temperature gradients within the film. Mass transfer at the interface is also expected to be independent of water flow rate if there is sufficient water present to uniformly wet the medium surface because the mass transfer rate is dependent on the saturated vapor pressure at the interface which depends only on the surface temperature. Based on visual observation, the medium appeared sufficiently wetted at all experimental flow rates; thus, the lack of dependence of the efficiency on flowrate is not surprising. In summary, when compared to larger, more complex evaporative cooling systems studied in the literature, our low-cost system behaves remarkably similarly, justifying its use in further preliminary laboratory studies as an alternative to higher cost systems. Further, the consistency of the air-side performance with complex pilot-scale systems demonstrates usefulness for classroom applications to allow students to gain a thorough understanding of performance trends associated with industrial equipment.

4.2 Time-dependent behavior of evaporative cooler under different operating conditions

Examination of the time-dependent temperature profiles during the factorial design experiments reveals an initial water-cooling regime, followed by a transition to air cooling for all experiments. Figures 4A and 4B show representative temperature profiles for water and air for experiments completed at a low values for water flow rate, air velocity, and initial water temperature and high values for the three parameters, respectively. For both conditions, the evaporative cooler initially operates in a water-cooling mode then transitions to an air-cooling mode after the water temperature reaches the inlet air temperature. Water and air-side temperatures continue decreasing, approaching the wet-bulb temperature of the inlet air (~11.5 °C). The time-dependent temperature profiles can be explained considering heat and mass transfer driving forces. In the initial region of the cooling profile, the water temperature is significantly greater than the incoming air, and high driving forces exist for heat and mass transfer. The surface temperature at the interface is much higher than the bulk air temperature, leading to a large temperature driving force for sensible heat transfer to the air. Sensible heat is transferred from the bulk-water, to the interface, to the bulk-air, leading to rapid water cooling. Further, the vapor pressure driving force for mass transfer is also maximized when the surface temperature is much higher than the bulk air temperature due to the exponential dependence of vapor pressure on temperature. Combined, both these phenomena lead to a high rate of cooling in the initial time regime as water is cooled and air is heated. As the water cools, the surface temperature approaches the bulk air temperature, leading to decreased driving forces for heat and mass transfer and declining cooling rates, evidenced by the non-linear temperature profiles. When the water temperature reaches the inlet air temperature, sensible heat is transferred from both the bulk air and water to the surface. In this regime, the surface temperature is lower than both the bulk air and bulk water temperatures due to the energy required for water vaporization which occurs even when the air and water temperatures are equal. Thus, due to latent heat associated with mass transfer at the interface the temperature at the interface is low and sensible heat transfer from the both the bulk air and bulk water towards the surface occurs. The cooling rate continues to decrease as water approaches the theoretical minimum wet-bulb temperature. At this point, there is little difference between the bulk-water and surface temperature, leading to minimal sensible heat transfer on the water side and a near-constant water temperature. Air is cooled significantly compared to the inlet temperature because of the large difference in the surface and bulk-air temperatures, giving a large driving force for sensible heat transfer towards the interface which is counterbalanced by latent heat required vaporize liquid to replace water vapor leaving as a results of the mass transfer driving force from the surface to the bulk air.

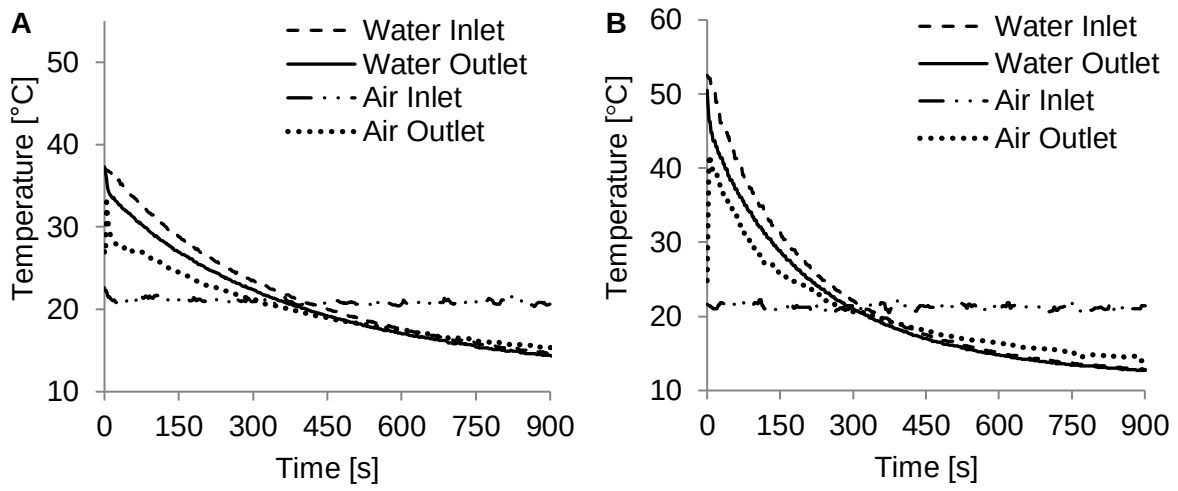

Figure 4. Temperature profiles of inlet and outlet water and air over a 15-min experiment for operating conditions of A) $\dot{V}_l$= 18.8 mL/s, $\bar{v}_{air}$= 0.4 m/s, T_i=37 °C and B) $\dot{V}_l$= 29.1 mL/s, $\bar{v}_{air}$= 1.0 m/s, T_i=53 °C

A closer examination of the temperature profiles reveals several key differences in the behavior. First, the initial rate of temperature change of the water is more rapid for a high flow rate, air velocity, and initial water temperature, indicating a higher initial cooling rate. The time required to reach the air-cooling regime and the final water and air-side outlet temperatures are lower for the experiment with a higher flow rate, velocity, and initial temperature at 300 s and 12.7 °C, respectively, compared to 375 s and 15.3 °C for a low flow rate, velocity, and initial temperature. Finally, the final air temperature also varies, 15.5 °C for low values of operating parameters and 14.6 °C for high values. These differences clearly suggest an impact of operating conditions on the heat and mass transfer phenomena occurring in the cooler, justifying further analysis to ascertain the effect of individual operating parameters and parameter interactions on the performance.

4.3 Experimental and predicted influence of individual operating parameters on rate and efficiency

Our numerical finite difference model has good predictive capability for the water-side outlet temperature, but is less accurate for predicting the outlet air conditions. This is clear in Figure 5 showing experimental and predicted outlet temperatures for the 20 factorial runs detailed in Table 1. The outlet water temperature is predicted with an average error of just 1.2 ± 1.0%, a maximum temperature difference of 1.6 °C, and a difference of less than 0.5 °C for 55% of the experiments, indicating good performance over a wide of conditions. As shown in Figure 5, the outlet water temperature varied significantly from 29.6 to 50 °C over the factorial runs, and differences in the outlet temperature were observed even for runs where the inlet temperature was equal, suggesting influences of water flow rate and air velocity on the outlet temperature, and thus, cooling rate and water-side efficiency. The air temperature was predicted slightly less accurately, but still with good agreement. The average error for air temperature prediction was 3.9 ± 2.6% with a maximum temperature difference of 4.0 °C. The larger discrepancy in outlet air temperature can be accounted for, at least in part, by our assumption that the air velocity, and thus, the mass flow rate of air used in the enthalpy balance, is constant throughout the packing. The air enthalpy balance is highly dependent on mass flow rate, calculated with the average air velocity. Air velocities were observed to be highly variable across the packing area and were difficult to measure, particularly at low fan voltages; thus, some the air velocities used in the model may not be highly accurate. Further, the sensible and latent heat transfer terms in the enthalpy balance are calculated based on average driving forces and correlations for flow past a single cylinder, which neglect effects of changes to heat and mass transfer driving forces in the direction of air flow as air flows sequentially across a number of cylinder banks.

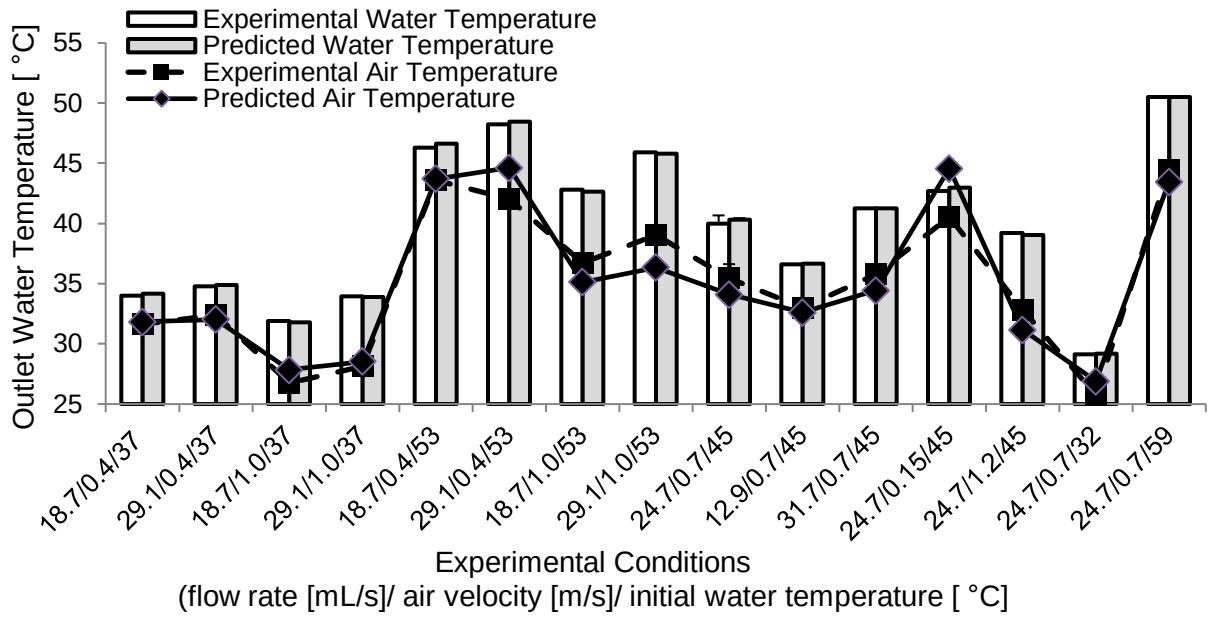

Figure 5. Measured and predicted water outlet temperatures at t = 8 s for each experiment. Values at 24.7 mL/s water flow rate, 1.5 m/s air velocity, and 45 °C are average values across six repeated center point runs.

Overall, the model predicts the outlet water temperatures highly accurately, and the outlet air temperatures with reasonable accuracy over a wide range of operating conditions with just a single adjustable fitting parameter representing the number of channels for water flow, not easily measurable given the complex geometry of the packing. The number of water channels was optimized at 200 in this study, approximately 60% of the maximum available locations for water flow given the dimensions of the packing used, but can be easily modified for other geometry and dimensions, giving flexibility.

As seen in Figure 6A, the initial cooling rate, which varied from 218-740 W, was predicted within 6.9 ± 8.1% with a maximum deviation on 34.9% predicted for Expt. 11 with the lowest tested air velocity. The minimum rate of 219 W was observed at operating conditions of 18.7 mL/s, 0.4 m/s, and 37 °C and maximum of 740 W observed at 29.1 mL/s, 1.0 m/s, and 53 °C, indicating a large influence of operating parameters. The initial rate was predicted within one experimental standard deviation, 23.9 W, calculated using the six replicated center point runs, for 60% of trials and within two standard deviations for 75% of trials. The water-side efficiency, which varied from 7.4 to 22.8%, was also predicted adequately by the model as seen in Figure 6B, with average and maximum deviations of 11.0 ± 10.3% and 33%, respectively, and values predicted within one experimental standard deviation for 70% of experiments. The minimum efficiency observed at 29.1 mL/s, 0.85 m/s and 37 °C and maximum of 22.8% observed at 18.9 mL/s, 2.2 m/s and 53 °C.

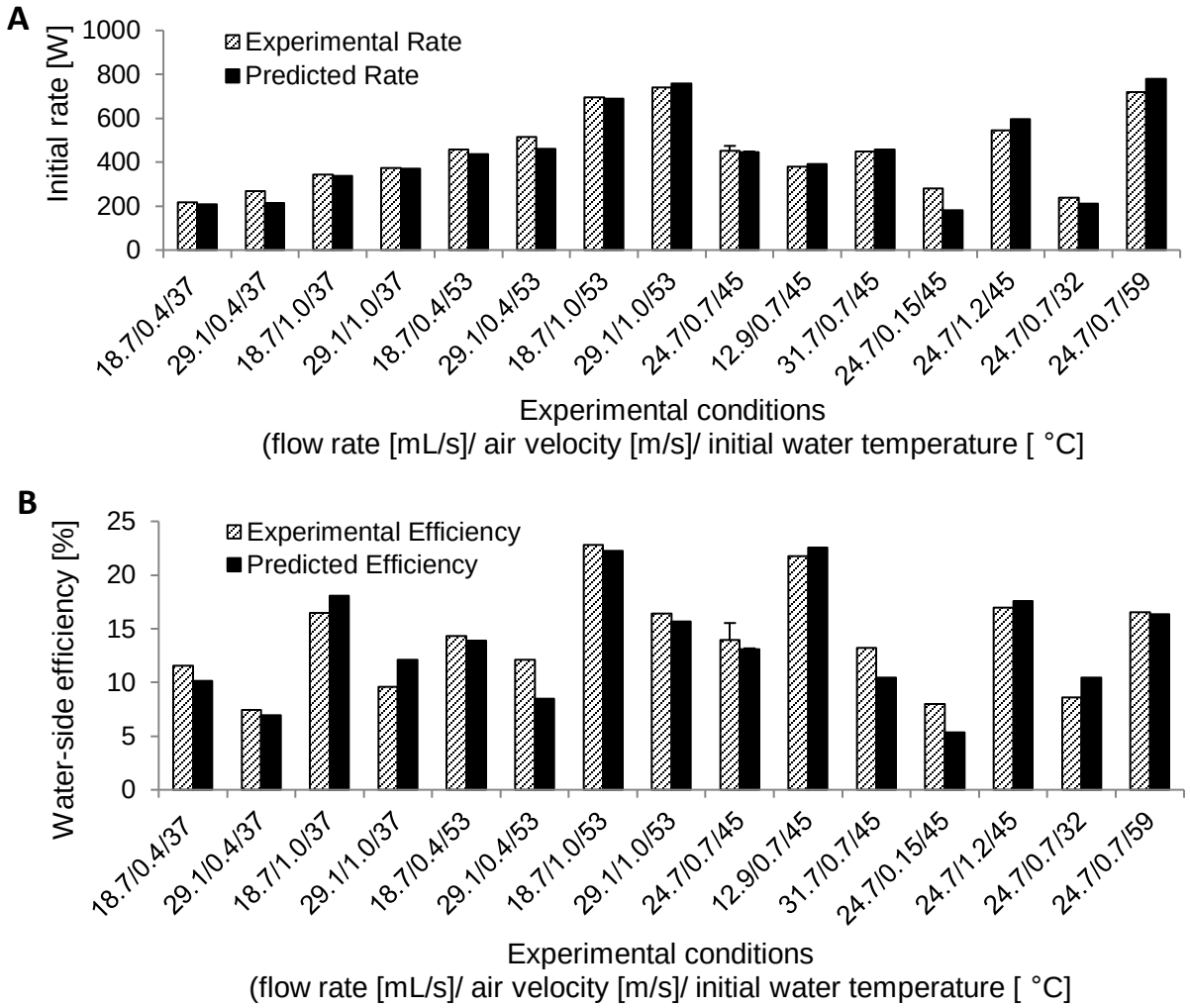

Figure 6. Predicted and measured initial cooling rates (A) and water-side efficiencies (B) for each factorial run

Taken together, the predicted outlet temperature, initial rate, and efficiency values obtained with the model suggest excellent predictive power for performance over a wide range of conditions. The numerical model was next used to elucidate individual effects of the flow rate, velocity, and initial temperature. Each factor was varied over the experimental range with other parameters fixed at the average conditions observed during factorial runs, as shown in Table 4.2.

Table 4. Input parameters for model calculations with varied flow rate, air velocity, and initial temperature

Varied parameter	Inlet air temperature	Inlet relative humidity	Initial water temperature	Water flow rate	Air velocity
Flow rate	21.5 °C	28.6%	44.7 ºC	**10-32 mL/s**	0.7 m/s
Air velocity	21.5 °C	28.6%	44.7 ºC	24.7 mL/s	**0.15-1.25 m/s**
Initial temperature	21.5 °C	28.6%	**30-60 ºC**	24.7 mL/s	0.7 m/s

Figures 7A, 7B, and 7C show the predicted and accompanying experimental data as a function of the water flow rate, air velocity, and initial water temperature on the initial rate of heat loss and efficiency, respectively. Just three experimental points are included in each figure, the three values along each center line in the fractional factorial

design, i.e., average values for the repeated central points, Experiments 15-20, and results at the minimum and maximum values for each factor, Experiments 9-14.

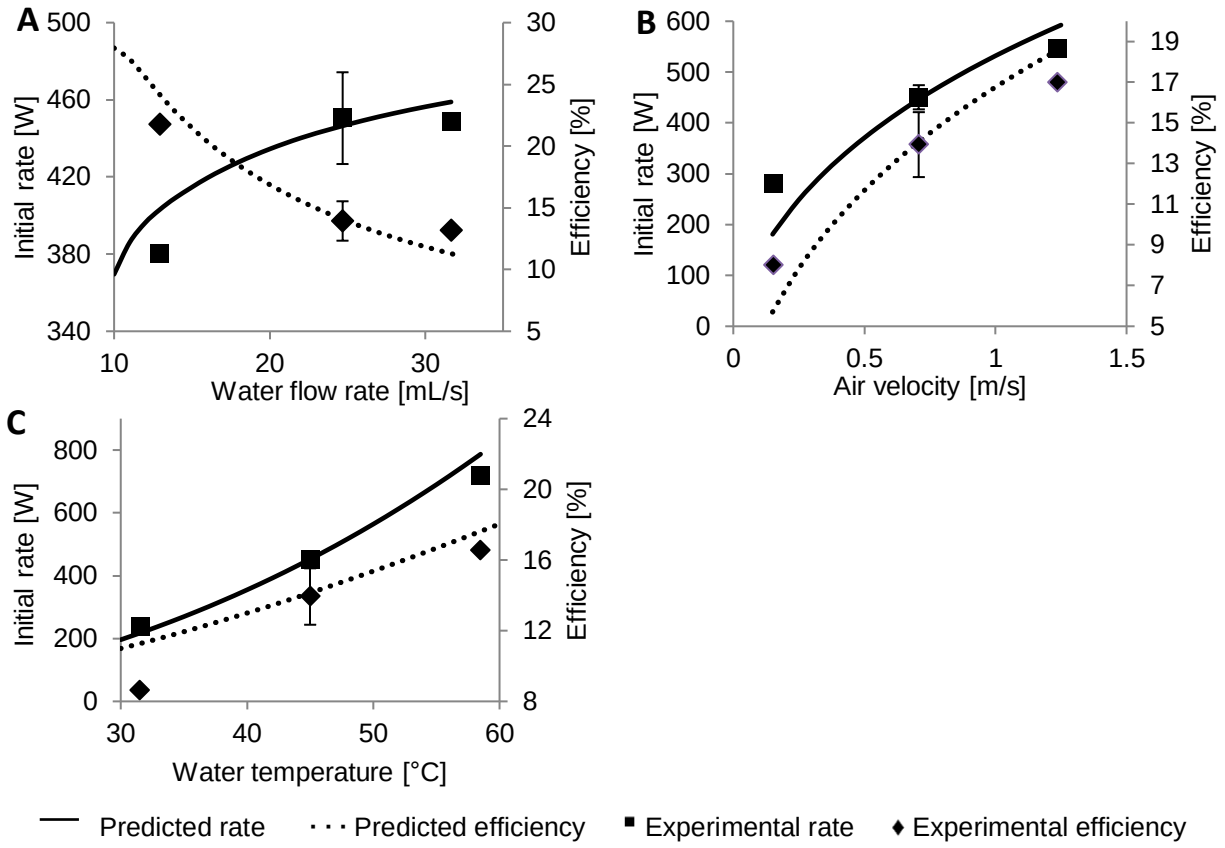

Figure 7. Predicted and experimental influences of water flow rate (A), air velocity (B) and initial water temperature (C) on the initial cooling rate and water-side efficiency.

Increasing the water flow rate has a non-linear, positive effect on the initial rate, but a negative effect on the efficiency with the rate increasing by 68.5 W over the experimental flow rate range and the efficiency decreasing by 8.6%. The air velocity and temperature have positive effects on both the rate and efficiency, with increasing air velocity resulting in non-linear increases in the rate and efficiency by 265 W and 9%, respectively, and the increasing initial water temperature resulting in increases of 531 W and 7.9%, respectively. The rates and efficiencies predicted with the numerical model matched experimental values within 102 W (37% error) and 2.7% (33% error), respectively, and non-linear influences of the water flow rate, air velocity, and initial water temperature on the rate and efficiency were predicted, which can be explained in light of heat and mass transfer driving forces. First, the convective heat transfer coefficient is shown through empirical correlations for flow around a cylinder to be non-linearly dependent on the air velocity as seen in Eqn. 3. As air velocity increases from 0.15 to 1.25 m/s, the convective heat transfer coefficient increases by 2.7-fold, corresponding to an increase to the sensible heat transfer rate at the air-water interface. Further, at the highest air velocity, the air temperature was shown to change by 14.1 ○C compared to 19.4 ○C at the lowest velocity, when all other process variables are held constant, suggesting a higher temperature driving force for convective heat transfer throughout the packing at high velocities. The influence of the initial water temperature on the rate and efficiency can also be explained in light of driving forces. The higher average surface temperature of 52.9 ○C predicted at an initial temperature of 58.5 ○C compared to a surface temperature of 29.8 ○C at an initial temperature of 31.5 ○C provides both a higher temperature driving force for convective heat transfer, dependent on the temperature difference between the bulk air and surface, as well as a higher driving force for mass and latent heat transfer through an increase to the vapor pressure at the surface

which itself has an exponential dependence on temperature. The difference in average surface temperature results in 3- and 3.4-fold increases in the temperature and vapor pressure driving forces for convective and latent heat transfer, respectively. Finally, the competing influence of water flow rate can be explained in light of the water temperature variation along the packing height and the contact time between the water and air. At high flow rates, the contact time between air and water is decreased, leading to a lower temperature change along the length of the packing and decreased efficiency. This is evidenced by a water temperature change of only 8.5% observed at a flow rate of 31.7 mL/s compared to a 14.6% decrease at a flow rate of 12.9 mL/s. However, the higher average temperature of the water along the medium at high flow rates provides a larger average driving force for heat transfer and mass transfer, resulting in a higher cooling rate. The non-linearity of the rate and efficiency as functions of the water flow rate can be explained by the fact that as the flow rate continues to increase, the water temperature will change minimally along the length of the packing, leading to a maximum rate and minimum theoretical efficiency.

The performance of the evaporative cooler is also consistent with results reported in existing literature for larger, more complex systems. Singh and Das [28] fit a 3rd-order polynomial regression function to data collected at a variety of water and air mass flow rates in a forced-draft evaporative cooler with wire mesh fill and found that efficiency non-linearly decreased with water flow rate while non-linearly increasing with air flow rate. Rahmati, Alavi, and Tavakoli [18] investigated the impact of water and air mass flow rate and initial water temperature in a counter-flow evaporative cooler with corrugated packing and found that the efficiency increased by approximately 15% with a 0.05 kg/s increase in the air mass flow rate, by 11% with a 0.04 m^3/h (11.1 mL/s) decrease in the water volumetric flowrate, and by approximately 6% with a 10 °C increase to the water temperature. Gao, et. al. [19] report an approximately 18% increase in efficiency with a 15 °C increase in temperature and a 7.5% decrease in efficiency with a 66 mL/s increase in water flow rate under conditions with no crosswind, and an approximately 1% increase in efficiency with a small 0.3 m/s increase to the crosswind velocity. Lemouari and Boumaza [29] report consistent increases in the heat rejection rate in a counterflow cooling tower with Vertical Grid Apparatus type packing with increases in the water mass flow rate and air mass flux for several water temperatures, as well as a positive effect of increased water temperature. Kong, et.al. [30] report non-linear increases of approximately 80% in the heat rejection rate over water mass flow rates from 1.95-3.61 kg/s range for water temperatures of 32-38 °C range in a counterflow cooling tower with corrugated foam packing. Overall, the impacts of flow rate, air velocity, and initial temperature on the water-side performance of the miniaturized evaporative cooler agree remarkably well with both theory and existing studies with larger scale laboratory testing apparatuses.

4.4 Fractional factorial design results for water-side performance

Response surface analysis reveals similar influences of individual operating parameters when compared to the numerical model predictions as well as several synergistic and antagonistic interactions between water flow rate, air velocity, and initial temperature on the performance of the evaporative cooler. The identification of factor interactions is a major advantage of response surface studies compared to traditional studies where one factor is varied at a time because it allows a more complete understanding of the effect of each operating parameter in the presence of other influential factors [20]. Regression with backwards elimination was used to develop models for both the initial cooling rate and water-side efficiency. The coded regression coefficients and p-values for the significance of individual regression terms, the overall models, and model lack-of-fits are shown in Table 3. As predicted by the numerical model, the initial cooling rate was significantly and positively impacted by all three operating parameters. Quadratic terms and the interaction between the fan voltage and initial temperature were also significant, suggesting non-linear effects of each parameter and a synergistic interaction of air velocity and initial temperature. Comparing the magnitude of the first-order coefficients reveals that the influence of the pump voltage, or flow rate, on the initial rate was 4.7- and 7.8-fold smaller than the influences of the fan voltage, or air velocity, and initial water temperature, respectively. This is confirmed by experimental results and trends predicted with the numerical model; the rate increases by only 68.5 W over the range of experimental flow rates, but by 265.4 and 481.3 W over the range of air velocities and temperatures. As previously discussed, the large influence of temperature is not surprising, given its significant impact on the magnitude of both the convective heat transfer and

latent heat and mass transfer occurring at the interface. The non-linearity is expected due to the exponential dependence of the vapor pressure on temperature, which drives mass transfer and therefore impacts the cooling rate. Similarly, as previously discussed, the air velocity is expected to have a large, non-linear effect on the cooling rate due to the coupled effects of the non-linear increase of the convective heat transfer coefficient with velocity and the lower temperature change of the air at high velocities which provides a larger temperature driving force for convection. The positive coefficient for the interaction term between the fan voltage and temperature suggests enhancement of the initial cooling rate at high values of both factors. This can be explained, as previously discussed, by the fact that both velocity and water temperature impact the convective transfer rate. Variance of the initial temperature affects the temperature and mass transfer driving forces, while variance of the velocity affects the convective heat transfer coefficient. Only through an increase in both parameters can convective heat transfer, and thus the water cooling rate, be maximized.

Table 3. Regression and ANOVA Results for Initial Rate and Water-side Efficiency

Term	**Regression Coefficient**		**p-value**	
	Rate [W]	***Efficiency [%]***	***Rate [W]***	***Efficiency [%]***
Intercept	450	14.0	1×10^{-13}	6.9×10^{-11}
P_v	18.4	-2.44	0.008	2.1×10^{-5}
F_v	86.6	2.52	2.6×10^{-8}	1.6×10^{-5}
T_i	144	2.53	1.8×10^{-10}	1.6×10^{-5}
P_v^2	-10.2	1.16	0.09	0.004
F_v^2	-10.7	-0.60	0.08	0.09
T_i^2	12.5	-0.57	0.045	0.10
$P_v \cdot F_v$	1.5	-0.79	0.85	0.09
$P_v \cdot T_i$	-3.1	0.22	0.68	0.62
$F_v \cdot T_i$	34.1	0.79	9×10^{-4}	0.09
		Model	1.0×10^{-8}	1.6×10^{-5}
		Lack-of-fit	0.77	0.98

The water-side efficiency was also impacted by all three operating parameters, as predicted by the numerical model. Quadratic terms and the interactions between fan voltage and pump voltage, and fan voltage and temperature were also significant. The regression coefficients reveal approximately equally influential main effects, with a negative influence of increasing the pump voltage, or flow rate, and positive influences of the fan voltage, or air velocity, and temperature. The fundamental reasons for the positive effects of temperature and air velocity, as well as their interaction on the efficiency are similar to those previously discussed; at higher initial temperatures and air velocities convective heat and mass transfer is increased, leading to more efficient water cooling. As discussed in Section 4.3, increasing the water flow rate is expected to have a negative influence on the efficiency due to the reduced contact time for heat and mass transfer between water and air at higher flow rates. The antagonistic interaction between water flow rate and air velocity can be explained in light of previous discussion. The ideal condition for high efficiency is a combination of high contact time between water and air and high rates of convective heat transfer. This is indicated by the negative coded regression coefficient on the interaction term between the pump and fan voltage; if low or high values of both factors are used in combination, the efficiency will decrease. The ratio of water to air flow rate is also well-known to influence the efficiency of cooling towers, with a low ratio resulting in the highest efficiencies. This is shown, for example, by Fisenko and Petruchik [8] in a numerical study of a counterflow mechanical draft cooling tower where the efficiency was predicted to decrease by 22% when the water/air flow ratio was increased from 0.3 to 1, and experimentally by Gharaghezi, et.al. [13] who reported an approximately 25% decreases in efficiency over ratios of 0.33 to 1.16 for a counterflow evaporative cooler with two types of corrugated packing.

The final response surface equations and surface plots for the initial rate and efficiency, generated after backwards elimination of non-significant terms allow further examination of initial rate and efficiency trends as functions of the

three operating parameters and identification of optimal operating conditions. Regression equations are shown in Eqns. 23 and 24 in non-coded units. Exponential terms are a result of the flow rate unit conversion from input voltage to flow rate in mL/s, which were found to be logarithmically related after experimental calibration:

$$\dot{Q}[W] = 27.4 + 76.6e^{0.06\dot{V}} - 169\bar{v}_{air} - 9.1T_i - 7.6e^{0.11\dot{V}} - 112\bar{v}_{air}^2 + 0.2T_i^2 + 13.7\bar{v}_{air}T_i \quad (23)$$

$$\varepsilon_w\,[\%] = -0.7 - 7.5e^{0.06\dot{V}} + 11.5\bar{v}_{air} + 0.9T_i + 0.9e^{0.11\dot{V}} - 5.9\bar{v}_{air}^2 - 0.01T_i^2 + \bar{v}_{air}\left(0.3T_i - 2.2e^{0.06\dot{V}}\right) \quad (24)$$

Both models show good fits to the experimental data with average errors of 2.9 ± 1.9% for the cooling rate and 5.1 ± 4.7% for the efficiency. The rate model had an overall p-value of 7.1 x 10^{-11}, adjusted and predicted R^2 values of 98.3% and 97.3%, respectively, and a non-significant lack-of-fit with a p-value of 0.88. The efficiency model had an overall p-value of 3.3 x 10^{-6}, adjusted and predicted R^2 values of 91.8 and 90.4%, respectively, and non-significant lack-of-fit p-value of 0.98. The relative effects of temperature, flow rate, and air velocity are clearly evident in the surface plots shown in Figure 8: an increase in temperature causes a large upwards shift of the initial rate and efficiency, particularly at high air velocities. The water flow rate has a relatively small impact on the rate, only increasing by a predicted 61 W over the range of flow rates tested. The air velocity has a small predicted influence on the rate at the lowest temperature, with a 102 W increase over the range of air velocities at 31.5 °C compared to a 500 W increase over the same range at 58.5 °C. This clearly highlights the synergistic impact of the temperature and air velocity. As shown in Figure 8A, the initial cooling rate is maximized at 28.5 mL/s, 1.2 m/s and 58.5 °C with a predicted rate of 951 W. This combination of factors was tested in triplicate at similar ambient conditions and an initial rate of 932 ±3.7 W was observed, much higher than the previously observed maximum of 740 W observed during factorial experiments and within 20 W of the maximum predicted by the response surface equation. The maximum water-side efficiency of 31.6% is predicted at 12.9 mL/s, 1.2 m/s, and 58.5 °C. This combination was also tested experimentally in triplicate and an efficiency of 31.1 ± 0.1% was observed, again much higher than the maximum of 22.8% observed during factorial runs and close to the predicted maximum efficiency, suggesting good predictive power of the response surface equation.

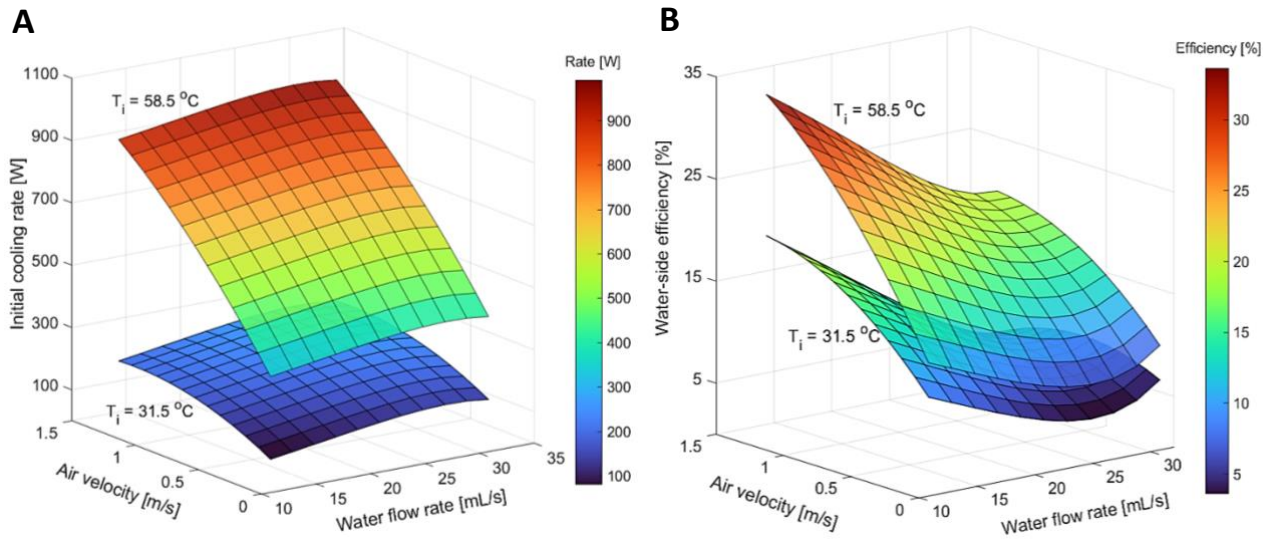

Figure 8. Response surface plots for initial cooling rate (A) and water side efficiency (B) as functions of water flow rate, air velocity at initial temperatures of 31.5 ºC (lower surfaces) and 58.5 ºC (upper surfaces).

Regression results reveal that the cooling rate and efficiency cannot be maximized simultaneously. Because of the relatively weak dependence of the cooling rate on water flow rate, a high rate of cooling may still be achieved at low

flow rates. Decreasing the flow rate from the optimum of 28.5 mL/s to 12.9 mL/s results in only a 7.1% decrease in the rate from 951 to 881 W, but a 59.8% increase in efficiency, from 19.8 to 31.6%. Thus, it is recommended that the evaporative cooler be operated at low flow rates, high air velocities, and high initial temperatures for the best overall performance. Response surface results provide a clear picture of the overall effects of each operating parameter on the evaporative cooler performance, which agree with results predicted by the steady-state numerical model, help to highlight several key interactions between factors, particularly the synergistic interaction between air velocity and initial temperature on the cooling rate, and allow identification of optimum conditions to maximize the rate and efficiency.

In summary, our intent of developing a miniature, inexpensive evaporative cooler suitable for testing packing materials and for demonstrating underlying principles to students has been met. Instructors may use the system to display both sensible and latent heat phenomena and first principles modeling of heat transfer effects taking place with confidence that resultant data will be consistent with predicted trends.

5. Conclusions

Herein, the development and characterization of a very low-cost, miniaturized direct cross-flow evaporative cooler is detailed. A simple steady-state finite difference model for the prediction of the water-side temperature profiles, outlet air conditions, and overall performance which accounts for temperature and velocity variations within the water film and makes use of empirical correlations to estimate the air-side heat and mass transfer coefficients is also presented. The numerical model, which may be palatable to undergraduate engineering students due to its simple nature, shows good agreement with measured water and air outlet temperatures, cooling rates, and efficiencies even with the inclusion of just a single, easily optimized fitting parameter. The performance of the evaporative cooler is evaluated over a wide range of water flow rates, air velocities, and initial water temperatures in a central composite fractional factorial design study, allowing the identification of synergistic and antagonistic interactions between operating parameters not often explored in the literature. Increases to the air velocity and temperature increase both the initial cooling rate and water-side efficiency, and a key synergistic interaction between the air velocity and initial water temperature is identified. Increasing the water flow rate is found to increase the initial rate but decrease the efficiency. Results obtained with the low-cost, miniaturized device agree remarkably well with experimental and numerical literature studies on larger-scale evaporative cooling towers and air-cooling devices. Thus, we conclude that the low-cost system and accompanying model will be useful for classroom applications, where it can be used to further students' understanding of the complex heat and mass transfer phenomena occurring during evaporative cooling, better preparing them to design and optimize industrial systems, and for use as a low-cost, simple alternative to traditional larger-scale experimental laboratory apparatuses for preliminary, rapid testing of new packing materials, packing orientations, and other novel aspects of evaporative cooler development.

Acknowledgements

This work was supported by National Science Foundation grant DUE 1821578. The authors acknowledge support from Eric Barrow of the Washington State University machine shop who assisted with prototype design and construction.

References

1. Cuce, P.M. and S. Riffat, A state of the art review of evaporative cooling systems for building applications, Renewable and Sustainable Energy Reviews, 54 (2016), pp. 1240-1249.
2. Foroushani, S., Misconceptions in engineering thermodynamics: A review, International Journal of Mechanical Engineering Education, 47/3 (2019), pp. 195-209.
3. Hands-on Activity Swamp Cooler, https://www.teachengineering.org/activities/view/cub_housing_lesson01_activity2, Accessed 27 April, 2022.
4. Chilling Science: Evaporative Cooling with Liquids, https://www.scientificamerican.com/article/chilling-science-evaporative-cooling-with-liquids/, Accessed 27 April, 2022.

4. Reynolds, O., et al., Development and implementation of a low-cost desktop learning module for double pipe heat exchange, Chemical Engineering Education, 56/2 (2021).
5. Beheshti Pour, N., et al., Ultra low-cost vacuum formed shell and tube heat exchanger learning module, International Journal of Engineering Education, 33/2A (2017). pp. 723-740.
6. Richards, C.D., et al., Implementation of very low-cost fluids experiments to facilitate transformation in undergraduate engineering classes, in 2015 ASEE Annual Conference & Exposition. 2015. Seattle, WA.
7. Kloppers, J.C. and D.G. Kroger, Cooling tower performance evaluation: Merkel, Poppe, and e-NTU methods of analysis, Journal of Engineering for Gas Turbines and Power, 127/1 (2005), pp. 1-7.
8. Fisenko, S.P. and A.I. Petruchik, Toward to the control system of mechanical draft cooling tower of film type, International Journal of Heat and Mass Transfer, 48/1 (2005), pp. 31-35.
9. Dai, Y.J. and K. Sumathy, Theoretical study on a cross-flow direct evaporative cooler using honeycomb paper as packing material, Applied Thermal Engineering, 22/13 (2002) pp. 1417-1430.
10. Kovačević, I. and M. Sourbron, The numerical model for direct evaporative cooler, Applied Thermal Engineering, 113 (2017), pp. 8-19.
11. Ibrahim, G.A., M.B.W. Nabhan, and M.Z. Anabtawi, An investigation into a falling film type cooling tower, International Journal of Refrigeration, 18/8 (1995), pp. 557-564.
12. Yan, M., et al., Experimental investigation on a novel arrangement of wet medium for evaporative cooling of air, International Journal of Refrigeration, 124 (2021), pp. 64-74.
13. Gharagheizi, F., R. Hayati, and S. Fatemi, Experimental study on the performance of mechanical cooling tower with two types of film packing, Energy Conversion and Management, 48/1 (2007), pp. 277-280.
14. Doğramacı, P.A. and D. Aydin, Comparative experimental investigation of novel organic materials for direct evaporative cooling applications in hot-dry climate, Journal of Building Engineering, 30/11 (2020), pp. 101240.
15. Sudprasert, S. and S. Sankaewthong, Utilization of rice husks in a water-permeable material for passive evaporative cooling, Case Studies in Construction Materials, 8 (2018), pp. 51-60.
16. Chen, X., et al., A novel evaporative cooling system with a polymer hollow fibre spindle, Applied Thermal Engineering, 132 (2018), pp. 665-675.
17. Tejero-González, A. and A. Franco-Salas, Optimal operation of evaporative cooling pads: A review, Renewable and Sustainable Energy Reviews, 151 (2021), pp. 111632.
18. Rahmati, M., R. Alavi, and M.R. Tavakoli, Experimental investigation on performance enhancement of forced draft wet cooling towers with special emphasis on the role of stage numbers, Energy Conversion and Management, 126 (2016), pp. 971-981.
19. Gao, M., et al., Experimental research of heat transfer performance on natural draft counter flow wet cooling tower under cross-wind conditions, International Journal of Thermal Sciences, 47/7 (2008), pp. 935-941.
20. Bezerra, M.A., et al., Response surface methodology (RSM) as a tool for optimization in analytical chemistry, Talanta, 76/5 (2008), pp. 965-977.
21. Ramakrishnan, R. and R. Arumugam, Optimization of operating parameters and performance evaluation of forced draft cooling tower using response surface methodology (RSM) and artificial neural network (ANN), Journal of Mechanical Science and Technology, 26/5 (2012) pp. 1643-1650.
22. Javadpour, R., S. Zeinali Heris, and Y. Mohammadfam, Optimizing the effect of concentration and flow rate of water/ MWCNTs nanofluid on the performance of a forced draft cross-flow cooling tower, Energy, 217/7 (2021), pp. 119420.
23. Hilpert, R., Wärmeabgabe von geheizten Drähten und Rohren im Luftstrom. Forschung auf dem Gebiet des Ingenieurwesens A, 4 (1933), pp. 215-224.
24. Geankoplis, C., Transport Processes and Separation Principles. 4 ed. 2003, New Jersey, USA: Prentice Hall.
25. Sheng, C. and G. Nnanna, Empirical correlation of cooling efficiency and transport phenomena of direct evaporative cooler, Applied Thermal Engineering, 40 (2012), pp. 48-55.
26. Wu, J.M., X. Huang, and H. Zhang, Theoretical analysis on heat and mass transfer in a direct evaporative cooler, Applied Thermal Engineering, 29/5-6 (2009), pp. 980-984.

27. Nada, S.A., et al., Experimental investigation of energy and exergy performance of a direct evaporative cooler using a new pad type, Energy and Buildings, 203/6 (2019), pp. 109449.
28. Singh, K. and R. Das, An experimental and multi-objective optimization study of a forced draft cooling tower with different fills, Energy Conversion and Management, 111 (2016), pp. 417-430.
29. Lemouari, M. and M. Boumaza, Experimental investigation of the performance characteristics of a counterflow wet cooling tower, International Journal of Thermal Sciences, 49/10 (2010), pp. 2049-2056.
30. Kong, Q.J., et al., Experimental investigation of the heat and mass transfer phenomena in a counterflow wet cooling tower with foam ceramic packing, Advances in Mechanical Engineering, 10/1 (2018).